Physics of Fluids

Modeling subgrid-scale scalar dissipation rate in turbulent premixed flames using gene expression programming and deep artificial neural networks

Cite as: Phys. Fluids **34**, 085113 (2022); https://doi.org/10.1063/5.0095886
Submitted: 13 April 2022 • Accepted: 11 July 2022 • Accepted Manuscript Online: 12 July 2022 • Published Online: 09 August 2022

C. Kasten, J. Shin, R. Sandberg, et al.

Physics of Fluids ARTICLE scitation.org/journal/phf

Modeling subgrid-scale scalar dissipation rate in turbulent premixed flames using gene expression programming and deep artificial neural networks

Cite as: Phys. Fluids **34**, 085113 (2022); doi: 10.1063/5.0095886
Submitted: 13 April 2022 · Accepted: 11 July 2022 ·
Published Online: 9 August 2022

C. Kasten,[1,a)] J. Shin,[1,2] R. Sandberg,[3] M. Pfitzner,[2] N. Chakraborty,[4] and M. Klein[1]

AFFILIATIONS

[1]Institute for Numerical Methods in Aerospace Engineering, Department of Aerospace Engineering, University of the Bundeswehr Munich, Neubiberg, Germany
[2]Institute for Thermodynamics, Department of Aerospace Engineering, University of the Bundeswehr Munich, Neubiberg, Germany
[3]Department of Mechanical Engineering, University of Melbourne, Parkville, Australia
[4]School of Engineering, Newcastle University, Newcastle, United Kingdom

[a)]Author to whom correspondence should be addressed: christan.kasten@unibw.de

ABSTRACT

In this present study, gene expression programing (GEP) has been used for training a model for the subgrid scale (SGS) scalar dissipation rate (SDR) for a large range of filter widths, using a database of statistically planar turbulent premixed flames, featuring different turbulence intensities and heat release parameters. GEP is based on the idea to iteratively improve a population of model candidates using the survival-of-the-fittest concept. The resulting model is a mathematical expression that can be easily implemented, shared with the community, and analyzed for physical consistency, as illustrated in this work. Efficient evaluation of the cost function and a smart choice of basis functions have been found to be essential for a successful optimization process. The GEP based model has been found to outperform an existing algebraic model from the literature. However, the optimization process was found to be quite intricate, and the SGS SDR closure turned out to be difficult. Some of these problems have been explained using the model-agnostic interpretation method, which requires the existence of a trained artificial neural network (ANN). ANNs are known for their ability to represent complex functional relationships and serve as an additional benchmark solution for the GEP based model.

I. INTRODUCTION

The scalar dissipation rate (SDR) plays a fundamental role in turbulent reacting, non-premixed,[1] partially premixed,[2] or premixed flames,[3–8] the latter being the focus of this work. The SDR signifies the local micro-mixing rate, which is influenced by turbulence, chemical, and molecular diffusion processes that are strongly coupled.[9] The instantaneous SDR of the reaction progress variable (RPV) c is defined as $N_c = D\nabla c.\nabla c$, where D is the diffusivity of RPV. The RPV c can be defined as $c = (Y_0 - Y)/(Y_0 - Y_\infty)$, where Y denotes the mass fraction of the species used for the definition of RPV, and the subscripts 0 and ∞ depict values in the unburned and fully burned gases, respectively. The present analysis focuses on the prediction of the subgrid scale (SGS) SDR $\widetilde{\epsilon}_c = \overline{\rho D \nabla c \cdot \nabla c}/\overline{\rho} - \widetilde{D}\nabla\widetilde{c}\cdot\nabla\widetilde{c}$, which appears explicitly in the transport equation of the SGS scalar variance $\sigma_v^2 = \widetilde{c^2} - \widetilde{c}^2$ transport equation,[10,11]

$$\frac{\partial(\overline{\rho}\sigma_v^2)}{\partial t} + \frac{\partial(\overline{\rho}\widetilde{u}_j\sigma_v^2)}{\partial x_j} = -\frac{\partial}{\partial x_j}\left[\overline{\rho u_j c^2} - 2\left[\overline{\rho u_j c} - \overline{\rho}\widetilde{u}_j\widetilde{c}\right]\widetilde{c} - \overline{\rho}\widetilde{u}_j\widetilde{c}^2\right] - 2\left[\overline{\rho u_j c} - \overline{\rho}\widetilde{u}_j\widetilde{c}\right]\frac{\partial\widetilde{c}}{\partial x_j} + 2\left[\overline{\dot{\omega}c} - \dot{\widetilde{\omega}}\widetilde{c}\right] + \frac{\partial}{\partial x_j}\left(\rho D\frac{\partial\sigma_v^2}{\partial x_j}\right) - 2\overline{\rho}\widetilde{\epsilon}_c. \quad (1)$$

Here, u_j denotes the jth component of the velocity vector and D and $\dot{\omega}$ represent the diffusivity and reaction rate of progress variable c, respectively. The knowledge of sub-grid scale (SGS) variance of reaction progress variable σ_v^2 is often necessary to construct the subgrid probability density function (PDF) of reaction progress variable of c in the context of flamelet[12,13] and Linear Eddy[14] based modeling methodologies, but the correct evaluation of σ_v^2 depends on the accurate closure of $\widetilde{\epsilon}_c$. Moreover, it has been demonstrated

previously[8,10,11,15,16] that in the flamelet regime (i.e., in the corrugated flamelets and thin reaction zones regimes[17]), the filtered reaction rate of reaction progress variable $\overline{\dot{\omega}}$ can be expressed using the Favre-filtered SDR as[8,10,11,15,16]

$$\overline{\dot{\omega}} = \{2\overline{\rho}\widetilde{N}_c/(2c_m - 1)\}\{1 - \exp(-\phi\Delta/\delta_{th})\} + f_1(\overline{\rho},\widetilde{c})\exp(-\phi\Delta/\delta_{th}), \quad (2)$$

where $\widetilde{N}_c = \widetilde{\epsilon_c} + \widetilde{D}\nabla\widetilde{c}\cdot\nabla\widetilde{c}$, $f_1(\overline{\rho},\widetilde{c})$ is a function such that $\dot{\omega} = f_1(\rho, c)$, and $\phi = 0.56\delta_{th}S_L/\alpha_{T0}$ is a model parameter with α_{T0} being the thermal diffusivity in the unburned gas. Equation (2) suggests that the accuracy of the prediction of the turbulent burning velocity $S_T = (\rho_0 A_p)^{-1}\int_V \overline{\dot{\omega}}\, dV$ (where ρ_0 is the unburned gas density and A_p is the projected flame area in the direction of mean flame propagation), and the heat release rate depends on the closure of $\widetilde{\epsilon_c}$ in the flamelet regime of combustion. This also serves as a motivation for considering the modeling of SGS SDR $\widetilde{\epsilon_c}$ for the flamelet regime of premixed combustion.[18] Several recent analyses concentrated on the statistical behaviors, modeling, and transport of SDR as well as the effects of flow topologies on SDR (see Ref. 19 and references therein). While large eddy simulation (LES) models for the SGS SDR are available (e.g., Ref. 8), the quantity is challenging to model, and new concepts might be helpful for finding high accuracy LES closures.

The availability of accurate and complete 3D datasets from direct numerical simulation (DNS) or experiment combined with the growing computing power has recently given a significant boost to the development of turbulence models[20,21] and combustion models[22–32] using machine learning (ML). Algorithmic innovations and advances in computer hardware have allowed the use of more complex algorithms that infer not just closure constants but also functional forms. Broadly speaking, ML studies can be split into two categories: those that are transparent and those that are not: methods like artificial neural networks (ANN) can represent very complex functional relationships but have to be treated as a black box by the user.[23,24] Diagnosing problems, ensuring physical constraints, and sharing models with the community are, thus, not always straightforward. For symbolic regression, such as gene expression programing (GEP),[33,34] the model inferred is a mathematical expression which has the advantage of producing a model as a function of key physical parameters, which can easily be implemented and ideally provides physical insights into the phenomenon of interest.[34–36]

Using a DNS database of statistically planar turbulent premixed flames, the focus of this work is to use ML methods to train a model for SGS SDR. While the focus lies on the application of GEP to the problem under consideration, ANN serves as an additional benchmark and provides explanations for the training behavior of GEP.

The rest of this paper is organized as follows. Sec. II introduces the DNS database and the data processing. Section III provides the details for the ML methods applied in this work. Results are shown and discussed in Sec. IV, and some final remarks and conclusions will close the paper.

II. DNS DATABASE

A subset of a DNS database[11,35] of turbulent premixed planar flames with single step Arrhenius type irreversible chemistry has been considered for the current analysis. In this context, the reaction rate $\dot{\omega}$ of reaction progress variable c takes the following form:

$$\dot{\omega} = B^*\rho(1-c)\exp\left[-\frac{\beta(1-T)}{1-\alpha(1-T)}\right], \quad (3)$$

where $\alpha = \tau/(1+\tau)$ and τ are the heat release parameters, B^* is the normalized pre-exponential factor, and β is the Zel'dovich number. The transport equation for the reaction progress variable c takes the following form:

$$\frac{\partial(\rho c)}{\partial t} + \frac{\partial(\rho u_i c)}{\partial x_i} = \dot{\omega} + \frac{\partial}{\partial x_i}\left[\rho D\frac{\partial c}{\partial x_i}\right]. \quad (4)$$

The database consists of six flames with global unity Lewis number Le, henceforth denoted as cases A-C. A second index L (H) is used for indicating a lower or (higher) heat release parameter, i.e., $\tau = 3.0$ ($\tau = 4.5$), where $\tau = (T_{ad} - T_0)/T_0$ with the adiabatic and unburned gas temperatures T_{ad} and T_0. The normalized turbulent root mean square (rms) velocity fluctuation u'/S_L, integral length scale to thermal flame thickness ratio l/δ_{th}, Damköhler number $Da = (lS_L)/(\delta_{th}u')$, Karlovitz number $Ka = (u'/S_L)^{3/2}(l/\delta_{th})^{-1/2}$, heat release parameter τ, and the Zel'dovich number β are shown in Table I. Here, S_L is the unstrained laminar burning velocity and δ_{th} is the thermal flame thickness. Standard values of Prandtl number ($Pr = 0.7$) and ratio of specific heats ($\gamma_g = 1.4$) have been used.

This DNS database has proven to be useful before[11,35,37–42] for testing and developing turbulent combustion models. Hence, the limited scale separation and parameter ranges of the present DNS database (inherent to all DNS datasets) should not be considered a limitation of the present study.

The turbulent velocity fluctuations and reacting flow fields are initialized using a homogeneous, isotropic velocity field in conjunction with a model spectrum suggested by Pope[43] and a steady, planar, unstrained premixed laminar flame solution, respectively. Flame–turbulence interaction takes place under decaying turbulence, and the simulation time is chosen to be larger than the chemical time scale as well as the eddy turnover time. The simulation domain is taken to be a cube of side length $45.8\,\delta_{th}$ and is discretized using a uniform Cartesian grid of 512^3 grid points. The ratio of integral scale to flame thickness is $l/\delta_{th} = 4.58$ (see Table I), which ensures at least ten turbulent eddies within the computational domain, such that their propagation is not affected by the periodic boundaries and such that enough samples can be obtained for collecting statistics. It can be seen from Table I that the Karlovitz number values of the cases considered in this analysis range from 5.23 to 27.16, which essentially means that these flames represent the thin reaction zones regime combustion according to Ref. 17. The Karlovitz number Ka can be scaled as $Ka \sim \delta_{th}^2/\eta^2$,[17] which suggests that the flame thickness remains greater than the Kolmogorov length scale in the thin reaction zones

TABLE I. Characteristic initial parameters for the planar turbulent premixed flames.

Case	u'/S_L	Da	Ka
AL/AH	5.0	0.92	5.23
BL/BH	9.0	0.51	12.62
CL/CH	15.0	0.31	27.16
$l/\delta_{th} = 4.58$, $\tau = 3.0$ and 4.5, $\beta = 6$			

regime, but the reaction zone thickness remains smaller than the Kolmogorov length scale. In DNS, both flame thickness (at least by ten grid points) and the Kolmogorov length scale in the unburned gas (at least by two grid points for the highest turbulence intensity) are sufficiently resolved, so the flame has a finite thickness. According to Ref. 44, premixed combustion in most industrial applications takes place under small and moderate values of the Karlovitz number. Furthermore, it was demonstrated in previous studies[18,19,45] that the statistical behaviors of the SDR and its evolution in premixed flames resemble the non-reacting mixing problems for very high Karlovitz numbers (e.g., $Ka > 100$). Thus, the SDR closure for very high Karlovitz numbers (e.g., $Ka > 100$) can be obtained using a single turbulent timescale associated with turbulent mixing.[8] Both facts serve as the motivation for the analysis of the sub-grid scale (SGS) SDR closure for moderate values of Ka.

Spatial derivatives for all internal grid points are evaluated using a tenth-order accurate central difference scheme, and time integration is carried out using an explicit third-order accurate low storage Runge-Kutta scheme. The boundary conditions in the mean flame propagation direction are taken to be partially nonreflecting, whereas boundaries in the transverse directions are periodic. More details on the database and numerical procedure can be found in Refs. 11 and 37. A thorough discussion regarding the simulation strategy and the validity of the simplifications in terms of chemistry for flame–turbulence interaction is reported in Refs. 46 and 47. Figure 1 exemplarily shows instantaneous isosurfaces of RPV for cases A and C.

To evaluate the SGS SDR, given by the expression $\widetilde{\epsilon}_c = \overline{\rho D \nabla c \cdot \nabla c}/\overline{\rho} - \widetilde{D}\nabla\widetilde{c}\cdot\nabla\widetilde{c}$ (where $\widetilde{q} = \overline{\rho q}/\overline{\rho}$ and $\overline{q}$ are the Favre-filtered and LES filtered values of a general quantity q, respectively, and ρ is the gas density), the DNS data have been explicitly filtered using a Gaussian filter kernel. Results will be presented from $\Delta \approx 0.4\,\delta_{th}$, where the flame is almost resolved, up to $\Delta \approx 5.6\,\delta_{th}$, where the flame becomes fully unresolved, and Δ is of the order of the integral length scale l.

The machine learning models introduced in Sec. III will be trained with cases AL, AH, BL, and BH and the filter widths $\Delta/\delta_{th} = 0.4$, 0.8, 1.2, 2.0, 3.6, 4.4, 4.8, and 5.6. Therefore, cases CL and CH are selected as test cases to examine the extrapolation capability in terms of the initial turbulence intensity, and the interpolation capability for the different filter widths by including $\Delta/\delta_{th} = 2.4$.

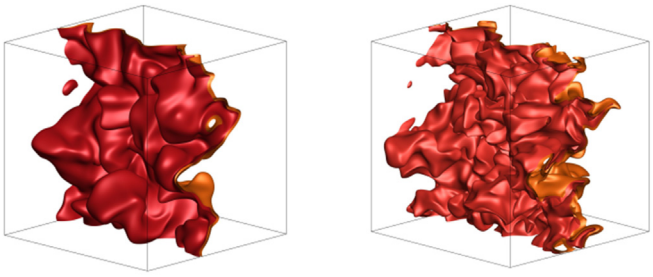

(a) (b)

FIG. 1. Instantaneous isosurfaces of RPV ($c = 0.3$, red and $c = 0.7$, orange) for cases AH (a) and CH (b).

III. METHODOLOGY

Sections III A–III C discuss briefly the strategies to close the SGS SDR term using a conventional algebraic LES-SDR model for premixed turbulent combustion,[7,8] GEP, and ANN. It is worth mentioning here that input parameters for all three methods are given by $\widetilde{c}$, Δ/δ_{th}, u'_Δ/S_L, and τ, and Ka_Δ and Da_Δ can be computed from this, while the single output parameter is the SGS SDR. The involvement of Δ/δ_{th} and u'_Δ/S_L in the input parameter also ensures that both mixing timescale Δ/u'_Δ and chemical timescale δ_{th}/S_L can be incorporated in the models enabled by GEP and ANN.

A. Algebraic SGS SDR closure

The model for the SGS part of the SDR for turbulent premixed flames (henceforth referred to as CS model) can be written as[7,8]

$$\widetilde{\epsilon}_c^{CS} = \frac{(1-f_b)\widetilde{c}(1-\widetilde{c})}{\beta_c} \times \left[2K_c^* \frac{S_L}{\delta_{th}} + (A^* - \tau Da_\Delta B^*)\frac{2u'_\Delta}{3\Delta}\right]. \quad (5.1)$$

Here, K_c^* is a thermo-chemical parameter ($=0.77\tau$ for these cases), $f_b = \exp\left[-0.7(\Delta/\delta_{th})^{1.7}\right]$ is a function that ensures that $\widetilde{N}_c$ approaches N_c when the flame is fully resolved (i.e., $\Delta \to 0$), and $Da_\Delta = \Delta S_L/u'_\Delta\delta_{th}$ is the SGS Damköhler number with $u'_\Delta = \left[\widetilde{(u_i u_i} - \widetilde{u}_i\widetilde{u}_i)/3\right]^{1/2}$ being the SGS velocity fluctuation. In Eq. (5.1), A^*, B^*, and β_c are the model parameters[8] with $Ka_\Delta = \left(u'_\Delta/S_L\right)^{3/2}(\Delta/\delta_{th})^{-1/2}$ and $c_m = \int_0^1 [\dot{w}c]_L f(c)dc / \int_0^1 [\dot{w}]_L f(c)dc$ being the SGS Karlovitz number and a thermochemical parameter ($=0.84$ for these cases), respectively, where $f(c)$ is the burning mode probability density function (PDF). The definitions of K_c^*, A^*, B^* and β_c are given as

$$\begin{aligned} K_c^* &= \frac{\delta_{th}/S_L \int_0^1 [\rho N_c \nabla\cdot\vec{u}]_L f(c)dc}{\int_0^1 [\rho N_c]_L f(c)dc}; \\ A^* &= 2.0\sqrt{Ka_\Delta}/\left(1.0+\sqrt{Ka_\Delta}\right); \\ B^* &= 1.2(1-\widetilde{c})^{0.2}/(1+Ka_\Delta)^{0.4}; \\ \beta_c &= \max\left\{\frac{2}{(2c_m-1)}, \left[\frac{1.05\tau}{\tau+1}+0.51\right]^{4.6}\right\}. \end{aligned} \quad (5.2)$$

B. Gene expression programing

The central aspect of GEP, being a particular evolutionary algorithm (EA), is to follow the Darwinian principle of natural selection called survival of the fittest.[48,49] GEP tries to find a functional representation of the SGS SDR using a set of variable operators and random numbers. Since introduced by Ferreira,[33] GEP has been used to solve all kinds of engineering problems and has been proven to work especially well for regression problems and, therefore, was chosen for this work.

The steps that are performed during the evolutionary progress are illustrated in Fig. 2, where steps 2 to 7b are repeated in every generation and steps 1 and 8 are only performed once. The GEP algorithm starts to create a (quasi) random initial population (1) of a predefined size. Afterward, the fitness values of all individuals are calculated (2) using the mean squared error between an individual's and the DNS

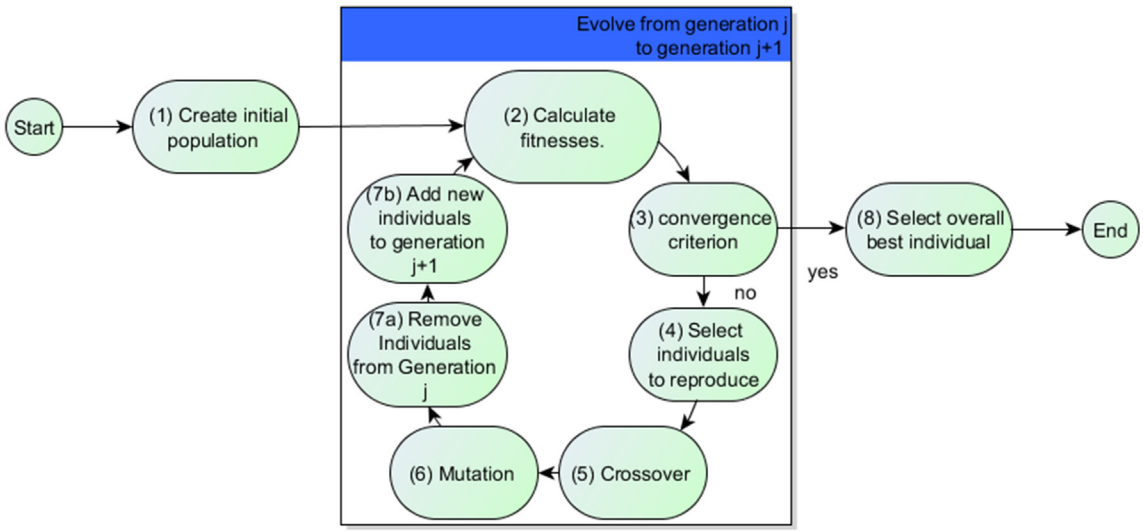

FIG. 2. Basic steps of a GEP algorithm.

function values. Then, it is checked if the one out of two convergence criteria is reached: (i) a squared error smaller than a predefined threshold ε or (ii) a given number of generations is reached. If one of these criteria is reached the best, overall individual will be presented (8). Otherwise, the individuals that are allowed to reproduce are defined (4) using a tournament selection with elitism. Consequently, the population is split into a predefined number of tournaments (100 for the run that found the presented model) with the same number (i.e., 100) of individuals being sampled randomly for each tournament. The individual with the best (smallest) fitness in a tournament wins and is allowed to reproduce, while the losers with the worst (biggest) fitness of these tournaments are replaced by the offspring. Reproduction is performed via one- or two-point-crossover (5), and each new individual has a certain probability (60% for the run that found the presented model) for each of its parts, which is selected randomly, to mutate (6) afterward. The mutation was setup in a way that every new individual has a 30% chance that any of its parts mutates. This translates into a mutation probability for any symbol of a chromosome of 30%/75 = 0.4%. The part that mutates is chosen randomly. The probability that two mates perform a one-point crossover was 50%, and that they perform a two-point crossover was 30%. For a detailed description on how crossover and mutation is performed for GEP-chromosomes, the reader is referred to Ref. 33. While the size of the population is fixed, some individuals must be removed (7a) to create space for the new individuals that are added to the population (7b) and get their fitness calculated (2). It is important to understand that the whole process (1)–(8) is repeated multiple times with different (about 200) random initial populations resulting in several "species," each with a best individual. Out of these winners, the most promising model candidates are finally selected. The present work makes use of a recent improvement of GEP, where the population is split into females and males in order to increase diversity.[50] Details are omitted here for the sake of brevity.

In GEP, the chromosome's string for each gene is divided into two parts:[33] a head with symbol length h and a tail with length t, subject to the relation $t = h(n_a - 1) + 1$, where n_a is the maximal number of arguments of all functions in the function set (here $n_a = 2$). In the present work, these parameters have been set to $h = 7$ and $t = 8$. Each individual is represented by five genes, resulting in a total length of 75. Due to the nature of GEP, not all these 75 symbols necessarily impact the encoded chromosome, which allows for variable length of the function expressions. As an example, consider the function set $F = \{+, -, \times, Q\}$, where Q indicates the square root, and the terminal set $T = \{a, b, c, 1\}$. For a gene with $h = 6$ and $t = 7$, the function with the highest arity has an arity of two, hence $n_a = 2$. The head may contain any symbol of both the function set F and the terminal set T, which includes the numerical constants, while the tail must only consist of symbols from the terminal set. Note that ephemeral random constants with an associated separate chromosome part, as described in Ref. 33, were not used in this work. The parsing tree in Fig. 3(a) encodes to the Pythagorean theorem $\sqrt{a^2 + b^2}$. The structure shown in Fig. 3(b) is commonly referred to as a gene. The chromosome of each individual can consist of several genes, which can be combined by any function with an arity of two. The relation between a GEP gene and its parsing tree is presented in Fig. 3, while in Fig. 3(b), the head and tail of the presented GEP gene are divided by a vertical line, which is only used for illustration. Note that the terminals after position 7 in Fig. 3(b) are not used to create the parsing tree and to encode the gene. For details on how a GEP gene is encoded into the parsing tree and how the parsing tree is translated into a function, the reader is referred to Ref. 33.

While, in this paper, only the best found individual of multiple runs with multiple random initial populations is presented together with its GEP parameters, several different configurations and combinations of crossover probabilities, etc., were tested during the course of this exercise. In general, diversity competes with selection pressure. Therefore, different selection pressure and diversity settings were tested by changing the optimization configuration. While a too high selection pressure (too low diversity) can lead to the optimization being stuck in a local optimum, a selection pressure too low (diversity too high) can lead to no convergence at all. Note that for the presented

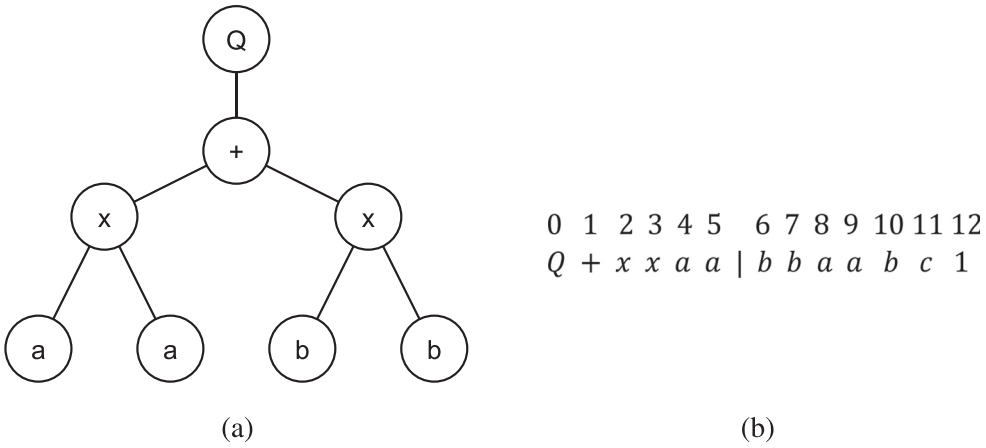

FIG. 3. GEP parsing tree (a) and corresponding GEP gene (b).

results, the tournament size, the mating size, and the mutation probability have the highest impact on selection pressure and diversity. With increasing the tournament size, the selection pressure increases while the diversity decreases since, the probability that an individual competes with the best individual (and loses again) increases.

The run where the presented GEP result was found had a population size of 1500 and was optimized for 15 000 generations. The presented model was found after about 8500 generations, and no better solution was found afterward.

C. Deep artificial neural networks

Deep ANNs have shown their capability to provide a successful surrogate model for predicting SGS terms for turbulent combustion problems.[23–25,51,52] Most of the previous studies have utilized convolutional neural networks which use learnable convolutional kernels that aim to seek the hierarchical topological features in the structured dataset.

In this current study, we employed the residual neural network (ResNet), that is, designed to perform complex and nonlinear regression tasks. The use of ResNet has allowed to achieve great accuracy on complicated datasets in the combustion community[25] and also diverse interdisciplinary areas.[53] It is also advantageous that it is applicable to unstructured meshes that are used by commercial CFD codes.

Figure 4 shows the schematic of the ResNet used in this study. The ResNet takes an input block to feed the input parameters to the neural network, and it ends with an output block to predict the output parameters. A ResNet block consists of three fully connected layers,

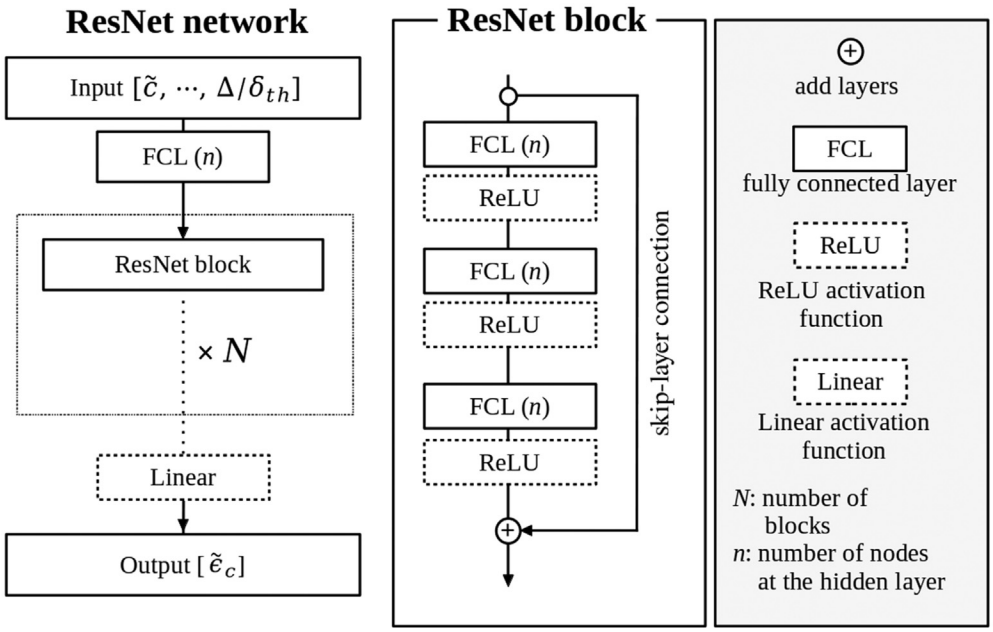

FIG. 4. Schematic of the deep neural network used in this study.

and each layer contains the ReLU activation function. To realize the residual skip connection, which is the key element of the ResNet, the skip-layer connection is concatenated from the start of the block to the end of the block, and then the linear activation function is added at the end of the neural network to satisfy the regression operability. The number of ResNet blocks N and the number of nodes at each hidden layer n are taken to 5 and 100, respectively. The total number of trainable parameters is approximately 170 000.

In the current contribution, feature importance analysis is considered to reveal the importance of the respective input parameter with respect to the output parameter, $\widetilde{\epsilon}_c$, in this study. Two methods are employed for this analysis: Shapley additive explanations (SHAP) and maximal information coefficient (MIC). The SHAP method offers model-agnostic interpretability of trained ANNs, based on the cooperative game theory.[54] The MIC method measures the relationship of two arbitrary parameters (i.e., how closely they are associated), by satisfying two statistical characteristics: generality and equitability.[55] These two methods are exploited to demonstrate the importance of the input parameters to be used for the GEP method. Details will be discussed in Sec. IV.

For the ResNet, the number of trainable parameters is 170 000, whereas for GEP, it is 75. Hence, it can be speculated that the current ResNet is more suitable for interpolating the data, while GEP provides the potential to reveal aspects of the underlying physics, in particular because of its transparency.

IV. RESULTS

Section IV A explains the chronology of steps taken for deriving a GEP model followed by a detailed discussion of the results and comparison with the ResNet model.

A. Deriving a model using GEP

GEP as described in Sec. III B was used to find a model expression for the SGS SDR using different basis functions and variables. The variable set consisted of $\widetilde{c}$, Da_Δ, Ka_Δ, Δ/δ_{th}, and τ, which was motivated by the existing model given in Eq. (5). It is worth noting that more variables could be included, like, for example, $|\nabla\widetilde{c}|$. As the number of possible variables is infinite and for the sake of an efficient training process, the aforementioned variables have been selected. The used function set is given by $[+, -, *, /, e^{\cdot}, \cdot^{x}, \sqrt{\cdot}]$ with the exponent in the range $x \in [2, 10]$. The fitness function f_i of individual i is given as

$$f_i = \sum_{cases}\sum_{\Delta}\sum_{data}\Delta\left(\widetilde{\epsilon}_c^i - \widetilde{\epsilon}_c^{DNS}\right)^2. \tag{6}$$

The fitness function f_i has been weighted with the actual filter width, which was used during *a priori* analysis of the DNS data, to increase the importance of larger filter widths, which are more relevant in terms of practical applications. Here, $\widetilde{\epsilon}_c^i$ and $\widetilde{\epsilon}_c^{DNS}$ denote the SGS SDR values of an individual's decoded chromosome (representing model candidate i) and the DNS values, respectively.

The first attempt for finding a model consisted of optimizing in physical space (i.e., 512^3 data points) by running simultaneously over different turbulence intensities, heat release parameters, and filter width combinations. It is remarked here that while filtering the DNS data does not reduce the dimension of the dataset, the optimization could be done on an arbitrary subset of the 512^3 cube at the price of losing samples. Such an approach has been discussed by Schöpplein *et al.*[56] but has not been tested in the context of this work. This made the fitness evaluation quite expensive, and, as a result, optimization for large population sizes and a large number of generations turned out to be economically unfeasible. The best models found using this approach were worse, in terms of the fitness value than the model given in Eq. (5). This was not only disappointing but also surprising, given the past success of GEP in approximating CFD closure terms[34–36] by using an integrity basis.

The second attempt involved finding a model expression for conditionally averaged $\widetilde{\epsilon}_c$ in the space of reaction progress variable $\widetilde{c}$, which has been discretized in 100 equally sized bins in the interval $[0, 1]$. Therefore, the inner sum in Eq. (6) had to be evaluated for only 100 data points instead of 512^3, which facilitated the use of larger population sizes and larger number of generations. The results became significantly better and comparable to the model presented in Eq. (5) since only the mean values in $\widetilde{c}$ space had to be learned. Nevertheless, GEP frequently got stuck in local optima.

These unsatisfactory results lead us to introduce a change of variables/basis functions, and GEP offers the possibility to use prior knowledge. Therefore, two polynomials $p(\widetilde{c})$ and $q(\widetilde{c})$ were introduced that roughly represent $\widetilde{\epsilon}_c$ for small (p) and large (q) filter with according to the DNS data presented later (see Fig. 8),

$$\begin{aligned} p &= -64.24\cdot\widetilde{c}\cdot(\widetilde{c}-0.6)\cdot(\widetilde{c}-0.8)\cdot(\widetilde{c}-1.0) \\ &\quad\times(\widetilde{c}^2-0.1256\cdot\widetilde{c}+0.015) \\ q &= 0.77\cdot\widetilde{c}\cdot(1.0-\widetilde{c}). \end{aligned} \tag{7}$$

The DNS results (see Fig. 8) indicate that $\widetilde{\epsilon}_c$ has four roots for small filter width $\widetilde{c} = 0.0, 1.0$ and approximately $\widetilde{c} = 0.6, 0.8$, which is reflected in the first part of p [i.e., $\widetilde{c}\cdot(\widetilde{c}-0.6)\cdot(\widetilde{c}-0.8)\cdot(\widetilde{c}-1.0)$], while the second part [i.e., $(\widetilde{c}^2-0.1256\cdot\widetilde{c}+0.015)$] is a polynomial with two imaginary roots that improves the shape of p without affecting the zeros. The large filter width contribution q represents the well-known expression proportional to $\widetilde{c}\cdot(1-\widetilde{c})$ from Eq. (5). The constant prefactors of p, q as well as the imaginary part of p have been found by linear regression. While the need for *a priori* knowledge can be considered a disadvantage, it enables a better training process. Furthermore, the ability to inform the machine learning algorithm with physical boundaries for large and small filter width can also be considered an advantage.

The feature importance map with respect to $\widetilde{\epsilon}_c$ for the input parameters $\widetilde{c}$, Da_Δ, Ka_Δ, Δ/δ_{th}, and τ as well as p and q is depicted in Fig. 5. MIC can deliver a quantitative measure if two variables, even

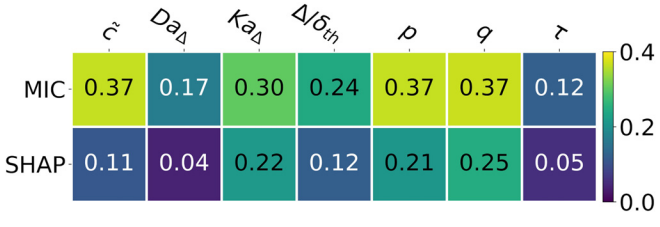

FIG. 5. Result of the feature importance analysis using MIC and SHAP. The values of MIC vary from 0.0 to 1.0, while the SHAP values add up to 1.0. A value of 1.0 (0.0) means perfectly associated (not associated).

with a nonlinear relationship, are closely related. As p and q are functions of $\widetilde{c}$, all three parameters result in the same MIC value. By contrast, the SHAP method (which requires a trained ANN) can investigate the partial contribution of the input parameters with respect to the objective parameter of the neural network, here $\widetilde{\epsilon}_c$. Interestingly, the SHAP method shows that p and q and Ka_Δ are the most influential parameters for predicting $\widetilde{\epsilon}_c$ among all parameters considered here. Consistent with this analysis, we found that, indeed, introducing p and q allowed us to spot better representations of SGS SDR $\widetilde{\epsilon}_c$.

With these basis functions, p and q, the optimization process could escape local optima more easily, and it became much easier for GEP to find individuals that represent $\widetilde{\epsilon}_c$ reasonably well for a wide range of filter widths. In fact, introducing these variables decreased the fitness values of the best-found individuals tremendously. Note that different GEP runs do not necessarily evolve to the same mathematical expression, while their functional output can still be similar. In general, the functional form and the performance of models from different runs differ, and one can either calculate an ensemble averaged model from all the trained models (or a subset of it) or, as in this work, simply select the best model according to the fitness function. Finally, a postprocessing step was added to ensure that the model fulfills physical constraints, namely, $\widetilde{\epsilon}_c^i \to 0$ for $\widetilde{c} \to 0, 1$, or $\widetilde{\epsilon}_c^i \to 0$ for $\Delta \to 0$. Moreover, division by zero should be avoided. The symbolic equation obtained from GEP for the normalized SGS SDR $\widetilde{\epsilon}_c^{GEP} \times \delta_{th}/S_L$ is given as

$$\begin{gathered}\widetilde{\epsilon}_c^{GEP} \times \delta_{th}/S_L = p \cdot e^{C_1} \cdot f(\Delta) + q\left(\sqrt{Ka_\Delta} - C_3\right) + \sqrt{Ka_\Delta} \cdot C_2, \\ \text{where } C_1 = -\widetilde{c}^{0.25}\left(\tau/\left(\Delta/\delta_{th} + 0.25\right)\right)^{-2.5}; \\ C_2 = \sqrt{7.8 \cdot 10^{-5} \cdot Da_\Delta^4 \cdot q}, \quad C_3 = \frac{0.019 \cdot e^{\left(\frac{p+q}{0.051^2 \cdot (Da_\Delta + \varepsilon)}\right)^{0.25}}}{\Delta/\delta_{th} + \varepsilon} f(\Delta); \\ f(\Delta) = 1 - e^{-3.5\frac{\Delta}{\delta_{th}}}, \quad \varepsilon = 10^{-3}.\end{gathered} \tag{8}$$

For Eq. (8), the physical constraints were fulfilled by introducing $f(\Delta)$ and by adding ϵ to avoid singularities. This possibility to analyze the model and to ensure physical and mathematical consistency of the model is a big advantage of GEP, which produces human readable results. In fact, this last step has even decreased the error further.

Figure 6 shows the mean squared error (top row) and the correlation coefficient (bottom row) between the model and DNS values, based on the parameters from physical space x (left column) and as well in the space of $\widetilde{c}$ (right column). It is especially worth noting that the GEP based model was only optimized using the conditional mean SDR values but still works reasonably well in physical space, which means that it can still predict local values.

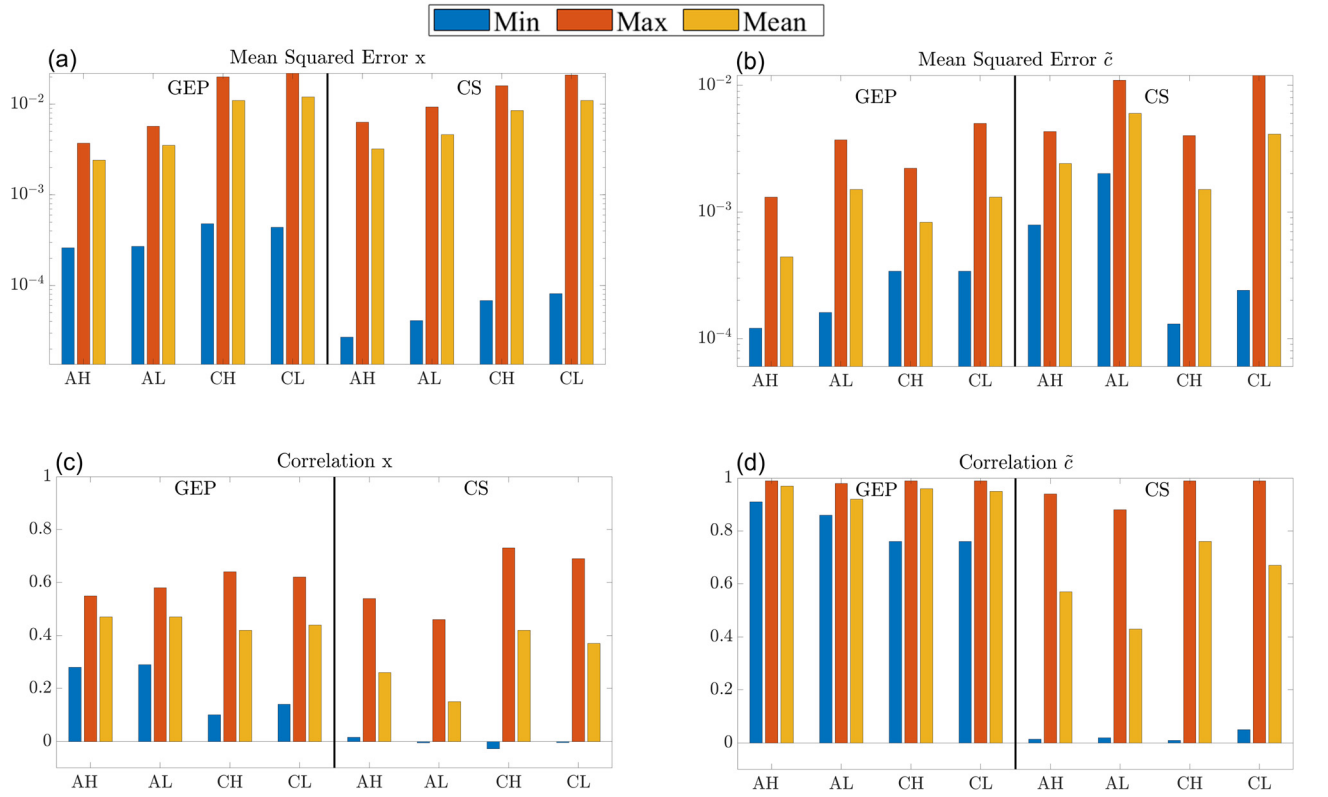

FIG. 6. Mean squared error [(a) and (b)] and correlation coefficient [(c) and (d)] between the model and DNS values, based on the parameters from physical space x [(a) and (c)] and in the space of $\widetilde{c}$(b and d). In each subfigure, results for the GEP based model (left) are compared to the existing CS model (right) shown in Eq. (5). All values are presented in the following manner: [min, max], mean, calculated as minimum, maximum, and mean over all filter width from 0.4 δ_{th} to 5.6 δ_{th} for that particular case.

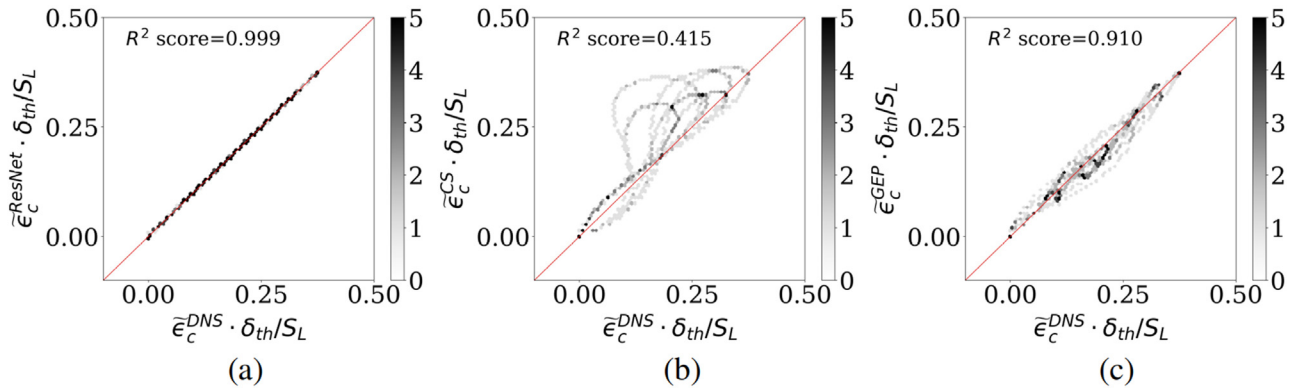

FIG. 7. Hexbin correlation plots for $\widetilde{\epsilon_c} \times \delta_{th}/S_L$ from DNS vs $\widetilde{\epsilon_c} \times \delta_{th}/S_L$ from ResNet (a), vs the prediction of the CS model [i.e., Eq. (5)] (b), vs the one from GEP (c) when $\Delta/\delta_{th} = 2.4$. Results consider all cases shown in Table I. The Hexbin plot shows the color of the frequency distribution of the points discretized onto the domain by 100×100.

B. Comparison of models from GEP and ANN

In order to demonstrate the predictive power of the GEP and ResNet models derived, the correlation plots of SGS SDR $\widetilde{\epsilon}_c$ computed by the models vs the one from DNS are depicted in Fig. 7, especially when $\Delta/\delta_{th} = 2.4$, which is the case the models were not trained on. Figure 7 shows that the results from the ResNet are in the best agreement with the DNS, showing a correlation coefficient of 0.999. The results computed from the GEP model also provide high correlations with the DNS, while the correlation strength deteriorates to some extent for the CS algebraic model [i.e., Eq. (5)].

Figure 8 shows the plots of SGS SDR $\widetilde{\epsilon}_c$ conditional on $\widetilde{c}$ for two cases AL and AH and the filter widths $\Delta/\delta_{th} = 0.8$ and 5.6 for the model was trained for, and together with the two cases CH and CL and the filter width $\Delta/\delta_{th} = 2.4$ for the model was not trained for.

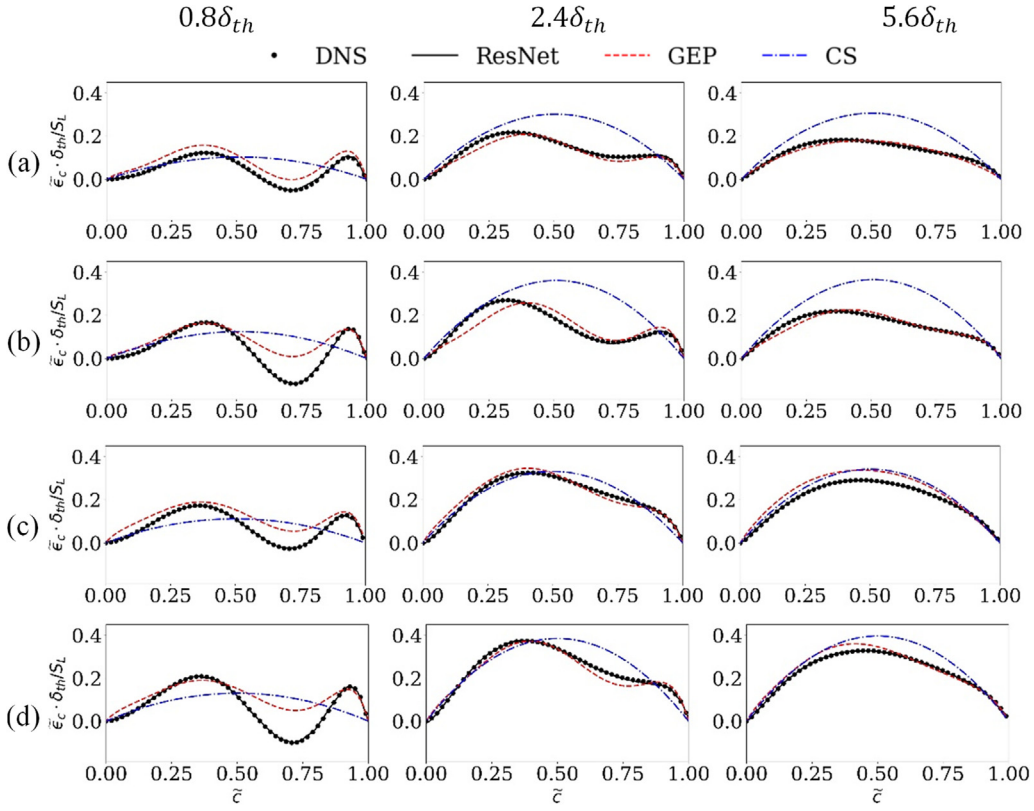

FIG. 8. Model prediction for normalized SGS SDR results (i.e., $\widetilde{\epsilon_c} \times \delta_{th}/S_L$) for cases (a) AL, (b) AH, (c) CL, and (d) CH, and the filter widths $0.8\delta_{th}$ (left), $2.4\delta_{th}$ (middle), and $5.6\delta_{th}$ (right).

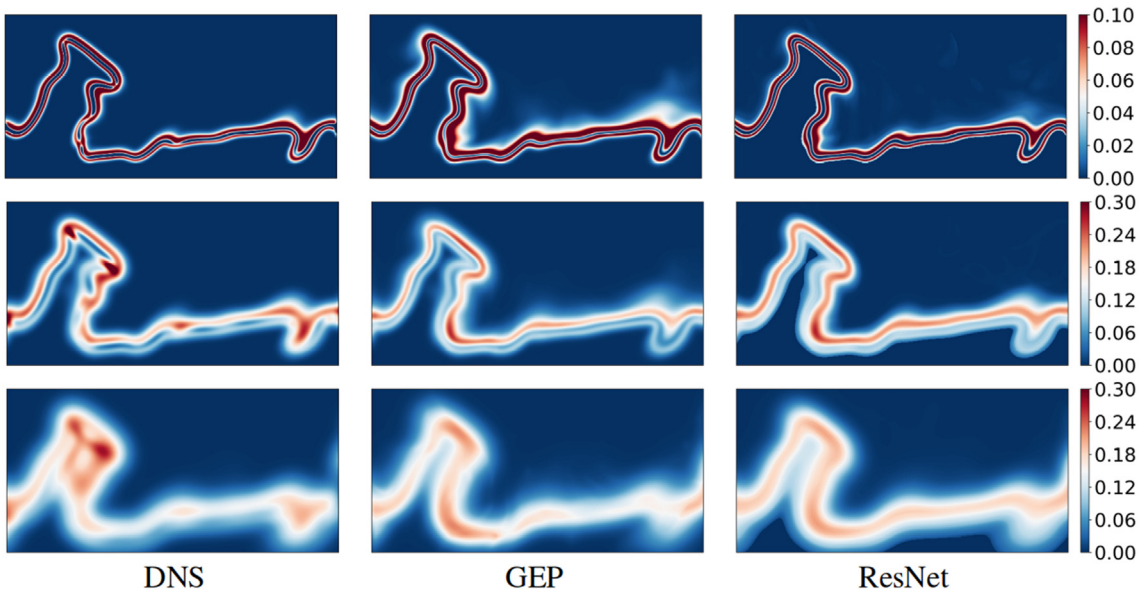

FIG. 9. Instantaneous distributions of $\widetilde{\epsilon}_c \times \delta_{th}/S_L$ computed from DNS, GEP, and ResNet shown in the x − y midplane for the filter widths $0.8\delta_{th}$ (top), $2.4\delta_{th}$ (middle), and $5.6\delta_{th}$ (bottom) for case AL.

It is important to note here that the quantity $\widetilde{\epsilon}_c$ can become negative for small filter width, which can be seen as follows: if one defines $c = \widetilde{c} + c''$ and assumes $\overline{\rho D} = const.$, the SGS SDR $\widetilde{\epsilon}_c = \overline{\rho D \nabla c \cdot \nabla c}/\overline{\rho} - \widetilde{D}\nabla\widetilde{c}\cdot\nabla\widetilde{c}$ can be written as $\widetilde{\epsilon}_c = \overline{\rho D}/\overline{\rho}\,\{(-\nabla\widetilde{c}\,\nabla\widetilde{c} - \nabla\widetilde{c}\nabla\widetilde{c}) + 2 - \nabla\widetilde{c}\nabla c'' + \overline{\nabla c''\nabla c''}\}$. For small filter width Δ (i.e., $\Delta < \delta_{th}$), the second and third terms are negligible, while the first term in parentheses, indeed, can become negative, and negative values of SGS SDR were obtained only for small filter widths in Fig. 8. For large filter widths (i.e., $\Delta > \delta_{th}$), the third term on the right-hand side (i.e., $\overline{\rho D}/\overline{\rho}\,\{\overline{\nabla c''\nabla c''}\}$) becomes the leading order contribution, and, thus, the SGS SDR assumes positive values.

It can be observed from Fig. 8 that ResNet and GEP models represent the SGS SDR well and very well, respectively, for different filter widths including cases and filter widths for which they were not trained for. Furthermore, it can be seen that the GEP model performs considerably better than the conventional algebraic model (i.e., CS model) for both large and small filter widths. Note that a moderate overprediction occurs for the GEP model for the smallest filter width, in particular for $\tau = 4.5$, close to the reaction zone (i.e., $\widetilde{c} \approx 0.7$), while the qualitative behavior is still captured well, especially compared to Eq. (5).

It should be emphasized that the ResNet model consists of several hundreds of thousand parameters. The GEP model, on the other hand, utilizes only a few parameters and mathematical operators, thus featuring a computational effort comparable to the CS algebraic model [i.e., Eq. (5)]. Figure 9 shows distributions of $\widetilde{\epsilon}_c$ computed from the DNS, GEP, and ResNet for filter widths $0.8\delta_{th}$, $2.4\delta_{th}$, and $5.6\delta_{th}$. It must be noted that a narrower field of view, showing only the flame front, has been selected. It can be clearly seen from Fig. 9 that GEP and ResNet models qualitatively and quantitatively show very good agreement with the DNS data for a large range of filter widths, including the validation data.

Finally, we would like to comment on the training and inference times for GEP and ResNet. The order of magnitude for the optimization time is about 3–4 days on 128 Cores for the present GEP model and about one day on a Titan X GPU for the ResNet. A direct comparison has to be done with care due to the entirely different hardware used. The inference times for the algebraic (CS), the GEP, and ResNet models are (normalized to the CS inference time) 1.0, 0.76, and 952.7, respectively. In fact, the GEP model is even slightly faster than the algebraic model, and both are three orders of magnitude faster than ResNet (it can be reduced to two orders of magnitude for inference using a GPU). As a general trend, the training time is faster for ResNet, but the inference time is larger compared to GEP.

V. CONCLUSIONS

The machine learning based modeling of SGS SDR of the reaction progress variable has been addressed in this work using an existing database of freely propagating statistically planar turbulent premixed flames with different turbulence intensities and heat release parameters. GEP has been used to infer a mathematical expression from the DNS dataset using the following chronology of steps. First, the model training has been conducted in physical space using local SGS SDR values, but the resulting model was found to be insufficient. In the second step, the model training has been performed in the space of the Favre-filtered reaction progress variable $\widetilde{c}$ by trying to represent the mean values of sub-grid scale SDR conditioned upon $\widetilde{c}$. This allowed for a more economic optimization process using a larger number of generations and resulted in better, but still not satisfactory

model performance. Finally, a change of basis function was found to improve the results substantially, and the resulting model clearly outperforms the CS algebraic model from literature. The feature importance analysis using the SHAP method based on a trained ANN also has proven that the change of the basis function was the enabling step for finding more accurate GEP models.

The prediction results from the models delivered by GEP and ANN show very good agreement with the DNS and outperform the algebraic model from literature. While ANN features an even better quantitative agreement than GEP, the GEP model represents a mathematical expression which is easy to evaluate and ensures physical consistency for $\widetilde{c} \to 0, 1$ or $\Delta \to 0$.

To the author's best knowledge, this is one of the first applications of GEP related to modeling SGS SDR, or more generally terms which are directly or indirectly important for closing the filtered reaction rate. It is also one of the few studies in the area of CFD where different machine learning methods are compared to each other, and this should be considered as the main achievement of the present research. It was not the scope of this work to find an expression for SGS SDR that works well in the most general scenarios of turbulent premixed combustion, and therefore, the limited scale separation and parameter ranges of the present DNS database (inherent to all DNS datasets) should not be considered a limitation of this present study. Nevertheless, further analysis with larger scale separation and higher Reynolds numbers, if possible, complemented by high fidelity 3D experimental data, will be needed for validation and refinement of the present models, which will form the basis of future investigations.

ACKNOWLEDGMENTS

This research was funded by dtec.bw—Digitalization and Technology Research Center of the Bundeswehr, project MORE, which we gratefully acknowledge. The computational support was provided by ARCHER (No. EP/R029369/1), CIRRUS, Leibniz Supercomputing Centre (Project No. pn69ga), and Rocket-HPC.

AUTHOR DECLARATIONS

Conflict of Interest

The authors have no conflicts to disclose.

Author Contributions

Christian Kasten: Software (lead); Visualization (equal); Writing – original draft (equal); Writing – review and editing (equal). **Junsu Shin:** Software (equal); Visualization (equal); Writing – original draft (equal); Writing – review and editing (equal). **Richard D. Sandberg:** Conceptualization (equal); Software (equal); Writing – review and editing (equal). **Michael Pfitzner:** Conceptualization (equal); Funding acquisition (equal). **Nilanjan Chakraborty:** Conceptualization (equal); Writing – original draft (equal); Writing – review and editing (equal). **Markus Klein:** Funding acquisition (equal); Supervision (lead); Visualization (equal); Writing – original draft (equal); Writing – review and editing (lead).

DATA AVAILABILITY

The data that support the findings of this study are available from the corresponding author upon reasonable request.

REFERENCES

[1]H. Pitsch and H. Steiner, "Scalar mixing and dissipation rate in large-eddy simulations of non-premixed turbulent combustion," Proc. Combust. Inst. **28**, 41–49 (2000).
[2]A. N. Karpetis and R. S. Barlow, "Measurements of flame orientation and scalar dissipation in turbulent partially premixed methane flames," Proc. Combust. Inst. **30**, 665–672 (2005).
[3]R. Bilger, "Some aspects of scalar dissipation," Flow Turbul. Combust. **72**, 93–114 (2004).
[4]N. Chakraborty, M. Champion, A. Mura, and N. Swaminathan, "Scalar dissipation rate approach to reaction rate closure," *Turbulent Premixed Flame*, 1st ed., edited by N. Swaminathan and K. N. C. Bray (Cambridge University Press, 2011), pp. 76–102.
[5]K. N. C. Bray, *Turbulent Reacting Flows*, edited by P. A. Libby and F. A. Williams (Springer Verlag, Berlin, Heidelburg, New York, 1980), pp. 115–183.
[6]N. Chakraborty and R. S. Cant, "Effects of Lewis number on flame surface density transport in turbulent premixed combustion," Combust. Flame **158**, 1768–1787 (2011).
[7]T. Dunstan, Y. Minamoto, N. Chakraborty, and N. Swaminathan, "Scalar dissipation rate modelling for large eddy simulation of turbulent premixed flames," Proc. Combust. Inst. **34**, 1193–1201 (2013).
[8]Y. Gao, N. Chakraborty, and N. Swaminathan, "Algebraic closure of scalar dissipation rate for large eddy simulations of turbulent premixed combustion," Combust. Sci. Technol. **186**, 1309–1337 (2014).
[9]N. Swaminathan and K. N. C. Bray, "Effect of dilatation on scalar dissipation in turbulent premixed flames," Combust. Flame **143**, 549–565 (2005).
[10]F. B. Keil, N. Chakraborty, and M. Klein, "Analysis of the closures of sub-grid scale variance of reaction progress variable for turbulent Bunsen burner flames at different pressure levels," Flow Turbul. Combust. **105**, 869–888 (2020).
[11]F. B. Keil, M. Klein, and N. Chakraborty, "Sub-grid reaction progress variable variance closure in turbulent premixed flames," Flow Turbul. Combust. **106**, 1195–1212 (2021).
[12]I. Langella and N. Swaminathan, "Unstrained and strained flamelets for LES of premixed combustion," Combust. Theor. Model. **20**, 410–440 (2016).
[13]I. Langella, N. Swaminathan, F. A. Williams, and J. Furukawa, "LES of premixed combustion in the corrugated-flamelet regime," Combust. Sci. Technol. **188**, 1565–1591 (2016).
[14]R. Ranjan, B. Muralidharan, Y. Nagaoka, and S. Menon, "Subgrid-scale modeling of reaction-diffusion and scalar transport in turbulent premixed flames," Combust. Sci. Technol. **188**, 1496–1537 (2016).
[15]T. Ma, Y. Gao, A. M. Kempf, and N. Chakraborty, "Validation and implementation of algebraic LES modelling of scalar dissipation rate for reaction rate closure in turbulent premixed combustion," Combust. Flame **161**, 3134–3153 (2014).
[16]D. Butz, Y. Gao, A. M. Kempf, and N. Chakraborty, "Large eddy simulations of a turbulent premixed swirl flame using an algebraic scalar dissipation rate closure," Combust. Flame **162**, 3180–3196 (2015).
[17]N. Peters, *Turbulent Combustion*, Cambridge Monograph on Mechanics (Cambridge University Press, Cambridge, 2000).
[18]N. Chakraborty, M. Champion, A. Mura, and N. Swaminathan, "Scalar dissipation rate approach to reaction rate closure," *Turbulent Premixed Flame*, 1st ed., edited by N. Swaminathan and K. N. C. Bray (Cambridge University Press, Cambridge, UK, 2011), pp. 74–102.
[19]N. Chakraborty, D. H. Wacks, S. Ketterl, M. Klein, and H. G. Im, "Scalar dissipation rate transport conditional on flow topologies in different regimes of premixed turbulent combustion," Proc. Combust. Inst. **37**, 2353–2361 (2019).
[20]K. Duraisamy, G. Iaccarino, and H. Xiao, "Turbulence modeling in the age of data," Annu. Rev. Fluid Mech. **51**, 357–377 (2019).
[21]H. Li, Y. Zhao, J. Wang, and R. Sandberg, "Data-driven model development for large-eddy simulation of turbulence using gene-expression programming," Phys. Fluids **33**, 125127 (2021).
[22]H. Pitsch and A. Attili, *Data Analysis for Direct Numerical Simulations of Turbulent Combustion* (Springer, Cham, Switzerland, 2020).
[23]F. C. Christo, A. R. Masri, E. M. Nebot, and S. B. Pope, "An integrated PDF/neural network approach for simulating turbulent reacting systems," Symp. (Int.) Combust. **26**, 43–48 (1996).

[24]Z. M. Nikolaou, C. Chrysostomou, L. Vervisch, and S. Cant, "Progress variable variance and filtered rate modelling using convolutional neural networks and flamelet methods," Flow Turbul. Combust. **103**, 485–501 (2019).
[25]J. Shin, Y. Ge, A. Lampmann, and M. Pfitzner, "A data-driven subgrid scale model in large eddy simulation of turbulent premixed combustion," Combust. Flame **231**, 111486 (2021).
[26]A. Ghani, I. Boxx, and C. Noren, "Data-driven identification of nonlinear flame models," ASME J. Eng. Gas Turbines Power **142**, 121015 (2020).
[27]S. Yao, B. Wang, A. Kronenburg, and O. T. Stein, "Conditional scalar dissipation rate modeling for turbulent spray flames using artificial neural networks," Proc. Combust. Inst. **38**, 3371–3378 (2021).
[28]M. McCartney, M. Haeringer, and W. Polifke, "Comparison of machine learning algorithms in the interpolation and extrapolation of flame describing functions," ASME J. Eng. Gas Turbines Power **142**, 061009 (2020).
[29]J. Ren, H. Wang, G. Chen, K. Luo, and J. Fan, "Predictive models for flame evolution using machine learning: A priori assessment in turbulent flames without and with mean shear," Phys. Fluids **33**, 055113 (2021).
[30]S. Yao, B. Wang, A. Kronenburg, and O. T. Stein, "Modeling of sub-grid conditional mixing statistics in turbulent sprays using machine learning methods," Phys. Fluids **32**, 115124 (2020).
[31]T. Readshaw, T. Ding, S. Rigopoulos, and W. P. Jones, "Modeling of turbulent flames with the large eddy simulation–probability density function (LES–PDF) approach, stochastic fields, and artificial neural networks," Phys. Fluids **33**, 035154 (2021).
[32]J. Ren, H. Wang, K. Luo, and J. Fan, "A priori assessment of convolutional neural network and algebraic models for flame surface density of high Karlovitz premixed flames," Phys. Fluids **33**, 036111 (2021).
[33]C. Ferreira, "Gene expression programming: A new adaptive algorithm for solving problems," Complex Syst. **13**, 87–129 (2001).
[34]J. Weatheritt and R. Sandberg, "A novel evolutionary algorithm applied to algebraic modifications of the RANS stress strain relationship," J. Comput. Phys. **325**, 22–37 (2016).
[35]M. Schöpplein, J. Weatheritt, R. Sandberg, M. Talei, and M. Klein, "Application of an evolutionary algorithm to LES modelling of turbulent transport in premixed flames," J. Comput. Phys. **374**, 1166–1179 (2018).
[36]M. Reissmann, J. Hasslberger, R. D. Sandberg, and M. Klein, "Application of gene expression programming to a-posteriori LES modeling of a Taylor Green vortex," J. Comput. Phys. **424**, 109859 (2021).
[37]M. Klein and N. Chakraborty, "A-priori analysis of an alternative wrinkling factor definition for flame surface density based large eddy simulation modelling of turbulent premixed combustion," Combust. Sci. Technol. **191**, 95–108 (2019).
[38]M. Pfitzner, J. Shin, and M. Klein, "A multidimensional combustion model for oblique, wrinkled premixed flames," Combust. Flame **241**, 112121 (2022).
[39]M. Pfitzner and M. Klein, "A near-exact analytic solution of progress variable and pdf for single-step Arrhenius chemistry," Combust. Flame **226**, 380–395 (2020).
[40]M. Hansinger, M. Pfitzner, and M. Klein, "Statistical analysis and verification of a new premixed combustion model with DNS data," Combust. Sci. Technol. **192**, 2093–2114 (2020).
[41]M. Klein, C. Kasten, and M. Germano, "Decomposition of turbulent fluxes from filtered data and application to turbulent premixed combustion modelling," Flow Turbul. Combust. **103**, 503–517 (2019).
[42]M. Klein, C. Kasten, and N. Chakraborty, "A-priori direct numerical simulation assessment of models for generalized sub-grid scale turbulent kinetic energy in turbulent premixed flames," Comput. Fluids **154**, 123–131 (2017).
[43]S. B. Pope, *Turbulent Flows* (Cambridge University Press, 2000).
[44]T. Poinsot and D. Veynante, *Theoretical and Numerical Combustion* (R.T. Edwards, Inc., Philadelphia, 2001).
[45]H. Kolla, J. Rogerson, N. Chakraborty, and N. Swaminathan, "Prediction of turbulent flame speed using scalar dissipation rate," Combust. Sci. Technol. **181**(3), 518–535 (2009).
[46]M. Klein, N. Chakraborty, and S. Ketterl, "A comparison of strategies for direct numerical simulation of turbulence chemistry interaction in generic planar turbulent premixed flames," Flow Turbul. Combust. **99**, 955–971 (2017).
[47]F. B. Keil, M. Amzehnhoff, U. Ahmed, N. Chakraborty, and M. Klein, "Comparison of flame propagation statistics extracted from direct numerical simulation based on simple and detailed chemistry. I. Fundamental flame turbulence interaction," Energies **14**, 5548 (2021).
[48]J. H. Holland, "Genetic algorithms," Sci. Am. **267**(1), 66–73 (1992).
[49]K. Man, K. Tang, and S. Kwong, *Genetic Algorithms: Concepts and Designs*, Advanced Textbooks in Control and Signal Processing (Springer, London, 2001).
[50]C. Kasten, J. Fahr, and M. Klein, "An efficient way of introducing gender into evolutionary algorithms," IEEE Trans. Evol. Comput. (published online 2022).
[51]M. Bode, M. Gauding, Z. Lian, D. Denker, M. Davidovic, K. Kleinheinz, J. Jitsev, and H. Pitsch, "Using physics-informed enhanced super-resolution generative adversarial networks for subfilter modeling in turbulent reactive flows," Proc. Combust. Inst. **38**, 2617–2625 (2021).
[52]C. Lapeyre, A. Misdariis, N. Cazard, D. Veynante, and T. Poinsot, "Training convolutional neural networks to estimate turbulent sub-grid scale reaction rates," Combust. Flame **203**, 255–264 (2019).
[53]C. Jiang, C. Jiang, D. Chen, and F. Hu, "Densely connected neural networks for nonlinear regression," arXiv:2108.00864 (2021).
[54]S. Lundberg and S.-I. Lee, "A unified approach to interpreting model predictions," in Proceedings of the 31st International Conference on Neural Information Processing Systems (2017), Vol. 30.
[55]D. N. Reshef, Y. A. Reshef, H. K. Finucane, S. R. Grossman, G. McVean, P. J. Turnbaugh, E. S. Lander, M. Mitzenmacher, and P. C. Sabeti, "Detecting novel associations in large data sets," Science **334**, 1518–1524 (2011).
[56]M. Schöpplein, J. Weatheritt, M. Talei, M. Klein, and R. D. Sandberg, *Application of an Evolutionary Algorithm to LES Modelling of Turbulent Premixed Flames* (Springer International Publishing, Cham, 2020), pp. 253–271.